Multiphysics computational fluid-dynamics (CFD) modeling of annular photocatalytic reactors by the discrete ordinates method (DOM) and the six-flux model (SFM) and evaluation of the contaminant intrinsic kinetics constants

Multiphysics Computational Fluid-Dynamics (CFD) Modeling of Annular Photocatalytic Reactors by the Discrete Ordinates Method (DOM) and the Six-Flux Model (SFM) and Evaluation of the Contaminant Intrinsic Kinetics Constants

Rodrigo PERALTA MUNIZ MOREIRA [*], Gianluca LI PUMA [*]

Environmental Nanocatalysis & Photoreaction Engineering, Department of Chemical Engineering, Loughborough University, Loughborough, United Kingdom

*Corresponding authors: Rodrigo PERALTA MUNIZ MOREIRA (r.peralta-muniz-moreira@lboro.ac.uk) and Gianluca LI PUMA (g.lipuma@lboro.ac.uk)

Highlights

- Annular photocatalytic reactor modeled by CFD and RTE-SFM or RTE-DOM
- Irradiance SFM boundary condition rather than fluence closely matches LVRPA by DOM
- RTE-SFM kinetics constants of 2-HBA closely match those determined by RTE-DOM

*Graphical Abstract (for review)

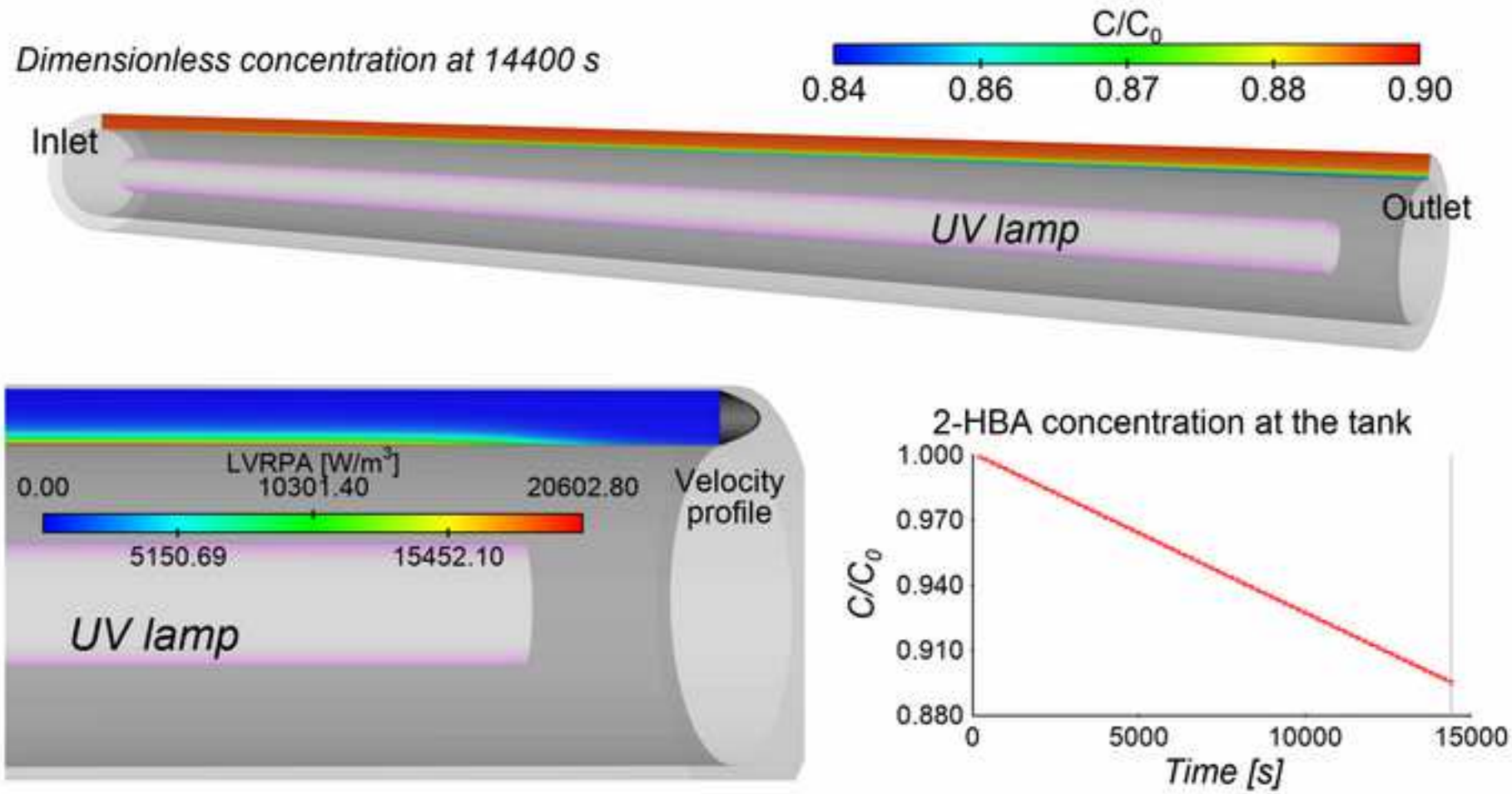

Multiphysics Computational Fluid-Dynamics (CFD) Modeling of Annular Photocatalytic Reactors by the Discrete Ordinates Method (DOM) and the Six-Flux Model (SFM) and Evaluation of the Contaminant Intrinsic Kinetics Constants

Rodrigo PERALTA MUNIZ MOREIRA *, Gianluca LI PUMA *

Environmental Nanocatalysis & Photoreaction Engineering, Department of Chemical Engineering, Loughborough University, Loughborough, United Kingdom

*Corresponding authors: Rodrigo PERALTA MUNIZ MOREIRA (r.peralta-muniz-moreira@lboro.ac.uk) and Gianluca LI PUMA (g.lipuma@lboro.ac.uk)

Abstract

Computational Fluid Dynamics (CFD) was used to model an annular photocatalytic reactor by solving the Radiative Transfer Equation (RTE) using the Discrete Ordinates Model (DOM) and the Six-Flux model (SFM) with isotropic scattering. The RTE boundary condition (BC) at the light entrance wall with the SFM was either the irradiance or the fluence rate, calculated using the LSSE, LSDE or ESDE light emission models. The Total Rate of Photon Absorption (TRPA) calculated with the SFM and fluence rate BC was overestimated by 29 - 21% in comparison to the DOM, when the optical thickness varied between 1.8 and 3.2%, and was underestimated by 3.1 - 8.8% when irradiance was the BC. The intrinsic reaction kinetics constants of 2-hydroxybenzoic acid (2-HBA) determined using the SFM in experimental reactors operated at very high optical thicknesses were 1% higher and 18% lower, than the constants determined with DOM, when irradiance or fluence rate, respectively, was used as BC. Overall, the SFM combined with the irradiance BC provides a more accurate evaluation of the LVRPA and intrinsic reaction kinetics constants, with

instantaneous solutions, while the DOM computational time > 20 min. This aspect is highly important in solar photocatalytic reactors with fluctuating irradiance.

Keywords: Annular photoreactor; Radiation Transfer Equation; Six-Flux model; Computational fluid dynamics; Intrinsic kinetics

1. Introduction

Heterogeneous photocatalysis has shown great potential as a remediation technology for the removal of pollutants from contaminated air, water and wastewater [1]. Despite numerous studies, industrial uptake and full-scale outdoor applications are still developing particularly due to the low quantum yield of photocatalysts [2]. Another possible reason for low use in industry is the complexity of large-scale system design and the need of simple methods for design, optimization and scale-up. Specifically, the design and modeling of photocatalytic reactors requires a complex analysis of the radiation field in the reactor [3, 4], which is governed by the absorption, scattering and emission, of photons by the catalyst. Then, the local rate of reacting species in photocatalytic aqueous suspensions is determined by combining the reaction kinetics with the radiation field and the fluid-dynamics in the reactor [5]. Uncoupling the contaminant reaction rate constants from the rate of photon absorption by the photocatalyst is also needed to allow reactor design and scale-up.

The radiation field in a photocatalytic reactor is computed by solving the radiation transfer equation (RTE), which yields the distribution of the radiation intensity in the reactor volume. After multiplication of the radiation intensity by the absorption coefficient and integration over the solid angle the Local Volumetric Rate of Photon Absorption (LVRPA) can be determined. Since the RTE is an integro-differential equation, a numerical method or an analytical approximation must be applied to compute the LVRPA. Among different computational methods [6], the most accurate are the Discrete Ordinate Model (DOM) [7, 8] and the Monte Carlo (MC) stochastic method [9, 10]. Despite the high accuracy, these models are often mathematically and computationally demanding [11], especially for systems where boundary condition fluctuates over time, such as in solar powered photocatalytic reactors [9].

Simplified approaches to compute the RTE include the Zero Reflectance Model [12], which is rather unrealistic since it neglects photon scattering, the Two-Flux Model [13], which assumes that photons travel in two directions (forward and backward), and the Six-Flux Model (SFM) [10], which assumes that photons are scattered through the six directions of the Cartesian coordinates. The advantage of these models is their capability to estimate the LVRPA using simple algebraic equations [14, 15].

The SFM provides the most accurate solution among the analytical approximation of the RTE, although it deviates from an exact solution. For example the irradiance transmitted through an annular photocatalytic reactor differs when the RTE is solved by SFM or DOM [8] and the accuracy of the SFM strongly depends on the nature of light emission source [11]. Moreover, the boundary condition used at the light entrance wall to solve the RTE with the SFM can have a significant impact on the accuracy of the SFM. Furthermore, the nature and geometry of the radiation source, such as direct or diffuse solar radiation or emission from artificial sources of radiation, influences the SFM accuracy.

The LVRPA is essential for calculating the reaction rate of water contaminants and the intrinsic kinetic constants [16], since these must be independent of the incident photon flux, wavelength, reactor geometry and volume. It is generally accepted that the rate depends linearly with the incident light flux under low radiation fluxes, but the dependence progressively shift to 0.5-order at high radiation fluxes [16]. Despite the limitations of the SFM, this model has been extensively used to model the photocatalytic oxidation of water contaminants [15, 17, 18, 19]. Coupling Computational Fluid Dynamics (CFD) with reaction kinetics and RTE modeling by DOM [5, 20] provides the most accurate modeling of photocatalytic oxidation of water contaminants, although the computational time using this method can be significant.

In this study, CFD was used to determine the intrinsic reaction kinetics constant of photocatalytic oxidation of 2-hydroxybenzoic acid (2-HBA) in annular flow-through photoreactors, solving the radiative transfer equation (RTE) using the DOM and the SFM, with isotropic scattering. The impact of the boundary condition (irradiance or fluence rate) used at the light entrance wall to solve the RTE with the SFM was investigated, to determine which of these boundary condition provides the most accurate estimation of the LVRPA in the reactor and of the intrinsic reaction kinetics constants of 2-HBA. This is important since numerical models as DOM and MC require a high computational effort in real reactor geometries, whereas the SFM solves the RTE in a simple algebraical way.

2. Methodology

2.1. Reactor geometry, operating conditions and experimental data

The photocatalytic oxidation of 2-HBA in an annular photocatalytic reactor [17] was selected for the validation of the models developed in this study and for the evaluation of the intrinsic kinetic constant of 2-HBA photocatalytic oxidation using suspensions of TiO_2 P25 photocatalyst. Table 1 summarizes the reactor and lamp dimensions for four different scenarios of reactor/light source dimensions, which were evaluated experimentally in another study [17] and modeled in this study. The outer wall of the annular photoreactor was made by a Pyrex glass tube with internal diameter equal to 54 mm and the inner wall of the reactor was a quartz tube with external diameter of 40 mm. A cylindrical lamp was housed inside the quartz tube at the centre of the reactor. The aqueous catalyst suspension circulated continuously through the annulus formed between the inner and outer walls of the photoreactor. The reactor was operated in the flow-through recirculation batch mode using a pulse-free peristaltic pump with the liquid recirculating through a well-mixed tank (2 L).

The optical properties of TiO_2 P25 as function of wavelength are shown in Fig. S1 (Supplementary Information, SI). For all modelling purposes, the spectral-averaged optical coefficients (Table 1) over the UVA and the UVB spectra intervals were used and these were calculated from Eqs. (1-2). The mass diffusivity of 2-HBA in water was estimated by Siddiqi-Lucas (1982) correlation (Eq. 3) where μ is the water viscosity in [cP], V_{2-HBA} is the molar volume of 2-HBA in [cm^3 mol^{-1}], V_w is the water molar volume in [cm^3 mol^{-1}], T is the temperature (298.15 K) and $D_{i,m}$ is the mass diffusivity of 2-HBA in water in [cm^2 s^{-1}].

$$\kappa^* = \frac{\int_{\lambda_{min}}^{\lambda_{max}} k_\lambda^* E_{p,\lambda}}{\int_{\lambda_{min}}^{\lambda_{max}} E_{p,\lambda}} \quad (1)$$

$$\sigma^* = \frac{\int_{\lambda_{min}}^{\lambda_{max}} \sigma_\lambda^* E_{p,\lambda}}{\int_{\lambda_{min}}^{\lambda_{max}} E_{p,\lambda}} \quad (2)$$

$$D_{i,m} = 9.89 \cdot 10^{-8} \mu^{-0.907} V_{2-HBA}^{-0.45} V_w^{0.265} T \quad (3)$$

Under the experimental conditions used to evaluate the intrinsic reaction kinetics constants of the photocatalytic oxidation of 2-HBA, the optical thicknesses of the catalyst suspension over the UVA and UVB regions ($\tau_{UVA} = 9.5$ and $\tau_{UVB} = 10.7$) were 10 times higher than that of the liquid solution ($\tau = 1.16$, for a decadic absorption coefficient equal to 3.591 M^{-1} cm^{-1} [22]), thus the absorption of photons by the 2-HBA solution was neglected in the model. It should be noted that the optimum optical thickness to operate a photocatalytic reactor using TiO_2 P25 should be around 1.8-3.0 [23] therefore the reactors in Table 1 were operated under conditions that strongly deviate from this optimum.

Table 1. (a) Evaluated scenarios, (b) operating conditions, (c) physicochemical properties and (d) optical properties.

(a) Evaluated scenarios

Reactor	Catalyst concentration [g/L]	Reactor length [mm]	Lamp length [mm]	Lamp radius [mm]	Irradiance at lamp wall in UVA spectrum (E_w)	Irradiance at lamp wall in UVB spectrum (E_w)

					[W/m^2] (†)	[W/m^2] (†)
A	1.0	600	550.0	7.75	34.6	29.7
B	2.0	600	550.0	7.75	34.6	29.7
C	1.0	300	213.0	7.75	6.5	6.5
D	1.0	300	213.0	7.75	89.4	0.0
(b) Operating conditions						
Flow rate ($\boldsymbol{Q}$) [L/min]						0.2 (†)
Initial contaminant concentration ($\boldsymbol{C_{2-HBA}}$) [mmol/L]						0.2 (†)
Tank volume ($\boldsymbol{V_{tank}}$) [L]						2.0 (†)
(c) Physico-chemical properties						
Density ($\boldsymbol{\rho}$) [kg m^{-3}]						998.2 (§)
Viscosity ($\boldsymbol{\mu}$) [cP]						1.003 (§)
2-HBA mass diffusivity in mixture ($\boldsymbol{D_{i,m}}$) [m^2 s^{-1}]						7.98·10^{-10} (#)
(d) Optical properties						
Specific absorption coefficient in UVA spectrum ($\boldsymbol{\kappa^*_{UVA}}$) [m^2 kg^{-1}]						189.9 (‡)
Specific absorption coefficient in UVB spectrum ($\boldsymbol{\kappa^*_{UVB}}$) [m^2 kg^{-1}]						508.5 (‡)
Specific scattering coefficient in UVA spectrum ($\boldsymbol{\sigma^*_{UVA}}$) [m^2 kg^{-1}]						1175.1 (‡)
Specific scattering coefficient in UVB spectrum ($\boldsymbol{\sigma^*_{UVB}}$) [m^2 kg^{-1}]						1016.1 (‡)
Scattering albedo in UVA spectrum ($\boldsymbol{\omega_{UVA}}$)						0.86 (‡)
Scattering albedo in UVB spectrum ($\boldsymbol{\omega_{UVB}}$)						0.67 (‡)

Notes: (†) Reported in reference [17]. The lamp irradiance was measured along the lamp length and its circumference using a spectral radiometer, and the results were averaged across both directions. (‡) Calculated from reference [17]. (§) Obtained from ANSYS Fluent database [21]; (#) Estimated from Eq. (3)).

2.2. Mathematical models

The flow in the annular reactor was considered laminar and incompressible (Re ~ 45). The mass and momentum conservation equations are:

$$\frac{\partial \rho}{\partial t} + \nabla \cdot (\rho \boldsymbol{u}) = 0 \tag{4}$$

$$\frac{\partial}{\partial t}(\rho \boldsymbol{u}) + \nabla \cdot (\rho \boldsymbol{u}\boldsymbol{u}) = -\nabla P + \nabla \cdot (\mu \nabla \boldsymbol{u}) \tag{5}$$

where $\boldsymbol{u}$ is velocity vector, P is the pressure, ρ and μ are the fluid density and viscosity, respectively.

The mass conservation of the generic i^{th} chemical species is obtained through the solution of Eq. (6-7):

$$\frac{\partial}{\partial t}(\rho Y_i) + \nabla \cdot \ (\rho \boldsymbol{u} Y_i) = \nabla \cdot \left(\rho D_{i,m} \nabla Y_i\right) + R_i \tag{6}$$

$$Y_N = 1 - \sum_{i}^{N-1} Y_i \tag{7}$$

where Y_i is the mass fraction of the i species, $D_{i,m}$ is the mass diffusivity of species i in the mixture, R_i is the mass source of species i in [kg m^{-3} s^{-1}] due to chemical reactions and N is the total number of chemical species present in the system.

2.2.1. Radiation Transport Equation

The RTE for an absorbing, scattering and emitting medium at the position $\vec{r}$ in the direction $\vec{s}$ is given by Eq. (8). The first term is the transport of the spectral radiation intensity I_λ, along the direction $\vec{s}$ and position $\vec{r}$, the second term is the radiation extinction in the $\vec{s}$ direction due to absorption and out-scattering, the third term is the radiation emission and the last term is the contribution from in-scattering from other directions. In this study, the scattering phase function $\Phi_\lambda(\vec{s} \rightarrow \vec{s}')$ was assumed as isotropic and emission was neglected.

$$\frac{dI_\lambda(\vec{r},\vec{s})}{ds} + (k_\lambda + \sigma_\lambda) I_\lambda(\vec{r},\vec{s}) = \varepsilon_\lambda I_{b,\lambda} + \frac{\sigma_\lambda}{4\pi} \int_0^{4\pi} I_\lambda(\vec{r},\vec{s}')\, \Phi_\lambda(\vec{s} \rightarrow \vec{s}') d\Omega' \tag{8}$$

Eq. 8 was solved using the DOM applied to a dual wavelength band interval [17], where the radiation spectrum was divided into UVA (315 nm to 400 nm) and UVB (280 nm to 315 nm) regions. In the DOM, each octant of the angular space 4π at any location was discretized into $N_\theta N_\phi$ solid angles, where θ and ϕ are polar and azimuthal angles, respectively. In two-dimensional calculations, a total of $4N_\theta N_\phi$ directions were discretized while $8N_\theta N_\phi$ directions were solved in 3D (for each wavelength band). Eq. (9) shows the RTE discretized by the DOM without the emission term.

$$\nabla \cdot (I_\lambda(\vec{r},\vec{s})\vec{s}) + (k_\lambda + \sigma_\lambda) I_\lambda(\vec{r},\vec{s}) = \frac{\sigma_\lambda}{4\pi} \int_0^{4\pi} I_\lambda(\vec{r},\vec{s}') \Phi(\vec{s} \rightarrow \vec{s}') d\Omega' \tag{9}$$

Then, the LVRPA [W m^{-3}] for each wavelength band was calculated by the integral of the radiation intensity over the 4π space multiplied by the absorption coefficient (Eq. 10):

$$LVRPA_\lambda = \kappa_\lambda^* c_{cat} \int_0^{4\pi} I_\lambda \, d\Omega \tag{10}$$

The Total Rate of Photon Absorption (TRPA) [W] corresponds to the power absorbed in the annular reactor and this was calculated integrating the LVRPA over the reactor volume:

$$TRPA_{\lambda} = \int_{V} LVRPA_{\lambda}\, dV \tag{11}$$

where λ in Eqs. (9-11) is replaced by the UVA or UVB spectral bands.

It should be noted that for aqueous solutions that show significant absorption in the UV region, the RTE must include a supplementary photon absorption term for the species in solution.

2.2.2. Six-Flux Model (SFM)

The discretization of Eq. (9) along the six cartesian coordinates yields the SFM [10]. The LVRPA calculated by the SFM for infinitely long annular photoreactor over a dimensionless radius, r^*, is given by:

$$LVRPA(r^*) = \frac{\tau_{app}\, E_0}{\omega_{corr}(1-\gamma)(1-\eta)R}\ \frac{\eta}{[\eta+(1-\eta)r^*]}\ \left[\left(\omega_{corr}-1+\sqrt{1-\omega_{corr}^2}\right)\ exp\left(-\tau_{app}r^*\right)+\gamma\left(\omega_{corr}-1-\sqrt{1-\omega_{corr}^2}\right)exp\left(\tau_{app}r^*\right)\right] \tag{12}$$

where E_0 is the incident photon flux, here investigated using either irradiance or fluence rate as boundary condition, R and R_{int} are the external and internal radius of the annular reactor, $\eta = R_{int}/R$ and a, b, ω_{corr} and γ are SFM parameters defined as follows

$$a = 1-\omega p_f - \frac{4\omega^2 p_s^2}{\left(1-\omega p_f-\omega p_b-2\omega p_s\right)} \tag{13}$$

$$b = \omega p_b + \frac{4\omega^2 p_s^2}{\left(1-\omega p_f-\omega p_b-2\omega p_s\right)} \tag{14}$$

$$\omega_{corr} = \frac{b}{a} \tag{15}$$

$$\gamma = \frac{1-\sqrt{1-\omega_{corr}^2}}{1+\sqrt{1-\omega_{corr}^2}}\, exp(-2\tau_{app}) \quad (16)$$

and τ, τ_{app} ω are the optical thickness, the apparent optical thickness and the scattering albedo defined as:

$$\tau = (\sigma^* + \kappa^*) c_{cat} R (1-\eta) \quad (17)$$

$$\tau_{app} = a\tau\sqrt{1-\omega_{corr}^2} \quad (18)$$

$$\omega = \frac{\sigma^*}{\kappa^* + \sigma^*} \quad (19)$$

For an isotropic scattering phase function the scattering probabilities over the forward, backward and side directions, p_f, p_b and p_s were equal to 1/6 [14]. The incident photons flux at the inner wall of the annular reactor, E_0, was estimated through three different models: line source spherical emission [24] (LSSE), in which the lamp is modeled as a line emitting radiation isotropically, line source diffuse emission (LSDE) [25], that assumes the lamp as a line emitting radiation diffusely, and extensive source superficial diffuse emission (ESDE) [26], where the lamp is modeled as a perfect cylinder and radiation is diffusely emitted by point emitters uniformly. The irradiance and fluence rate at the reactor light entrance wall were evaluated using these three models (see equations in SI).

2.2.3. Kinetic mechanism

The photocatalytic oxidation of 2-HBA was modeled by a pseudo Langmuir-Hinshelwood (L-H) kinetic rate equation (Eq. 20) as indicated in previous studies [17]. The dependence of the rate from the concentration of 2-HBA shifts from zero-order at high 2-HBA concentrations to first-order at low 2-HBA concentrations. Moreover, the reaction rate was proportional to the m^{th} power of the LVRPA. The contribution of the LVRPA [W m^{-3}] in the contaminant rate law was considered over a dual UVA and UVB band as shown in Grčić and Li Puma [17].

$$-r_{2-HBA} = \frac{k_1 K_{L-H}}{1 + K_{L-H} C_{2-HBA}} C_{2-HBA} \left[(LVRPA_{UVA})^m + (LVRPA_{UVB})^m \right] \quad (20)$$

where m equals 0.5 for moderate to intense photon fluxes [27], k_1 [kmol m^{-1} s^{-1} $W^{-0.5}$] is the intrinsic kinetic constant of photocatalytic oxidation of 2-HBA, K_{L-H} [m^3 $kmol^{-1}$] is the Langmuir-Hinshelwood binding constant for TiO_2 P25, C_{2-HBA} [kmol m^{-3}] is the concentration of 2-HBA.

2.3. Numerical procedure

ANSYS Fluent R2019 axisymmetric solver was used to solve the reacting flow. Two numerical domains were generated: the air gap between the lamp and the inner wall of the reactor (zero photon absorption) and the TiO_2 suspension region (the optically thick region). The computational mesh (Fig. S2, SI) generated in ANSYS Meshing software was made by 90,000 elements. The number of polar divisions and azimuthal divisions in the DOM were 12 and 4, respectively, in order to achieve the independence from the angular discretization. A lower discretization in the azimuthal direction was sufficient since the model was in 2D. In summary, 382 coupled partial differential equations were solved in the DO model (i.e., 192 per wavelength band).

The boundary conditions to solve the RTE with the DOM in ANSYS Fluent were: (a) diffuse emission uniformly distributed on the lamp surface; (b) transparent inner wall with specular transmission and zero emissivity; (c) fixed temperature of 1 K and emissivity of 1 at the outer wall.

The solution of the fluid flow and the radiation field in the numerical procedure were independently calculated and the results were combined with the material balance of the reacting species in the reactor to calculate the 2-HBA degradation rate. The fluid flow in the annular reactor was assumed at steady-state and the applied boundary conditions were: d)

inlet parabolic velocity profile given by Eq. (21); e) outlet fixed relative pressure (0 Pa); f) no fluid slip at walls; g) frozen velocity field at the air gap between lamp and inner wall.

The laminar fluid velocity along the z-coordinate was modeled by:

$$u_z = \frac{2Q}{\pi R\left[(1-\eta^4) - \frac{(1-\eta^2)^2}{\ln(1-\eta)}\right]}\left[1-(r/R)^2 + \frac{1-\eta}{ln(1/\eta)}ln(r/R)\right] \quad (21)$$

where $\eta = R/R_{int}$ and r is the radial coordinate. A scheme of the numerical domain and boundary condition is shown in Fig. S3 in SI.

The transport equation for 2-HBA (Eq. 6) was solved under transient conditions, and the concentration at the reactor outlet, $C_{2-HBA,\ out\ reactor}$, was calculated by averaging the radial volumetric flow rate over the annular space.

$$C_{2-HBA,\ out\ reactor} = \frac{1}{Q}2\pi\int_{R_i}^{R} r\ u_z\ C_{2-HBA}\ dr \quad (22)$$

The concentration of 2-HBA at the reactor inlet (equals to the concentration at the tank outlet, $C_{2-HBA,\ out\ tank}$) varied with time and this was calculated by solving the mass balance around the recycling tank:

$$V_{tank}\frac{dC_{2-HBA,out\ tank}}{dt} = Q\left(C_{2-HBA,\ \ out\ reactor} - C_{2-HBA,\ out\ tank}\right) \quad (23)$$

where V_{tank} is the tank volume, Q is the flow rate.

Eq. (20, 22-23) were solved with User-Defined Functions defined in ANSYS Fluent after calculating the LVRPA either by the DOM describe in section 2.2.1 or importing the algebraic solution of the SFM. The numerical method convergence criterion was taken as minimum residuals below $1{\cdot}10^{-6}$. The time step adopted for the transient simulations was 10 seconds, however, lower time steps were evaluated to ensure that the result was independent on the time-step size adopted (data not shown).

The CFD model was coupled with the optimization software Dakota, version 6.5, to estimate the intrinsic kinetics constants of the degradation of 2-hydroxybenzoic acid in

annular photocatalytic reactors of Table 1. The kinetic estimation was achieved by minimizing the objective function:

$$F_{obj} = \min\left\{\sum_{i=1}^{I}\sum_{j=1}^{J}\left(C_{2-HBA,i,j}^{\exp} - C_{2-HBA,i,j}^{CFD}\right)\right\} \quad (24)$$

where I and J are the number of samples ($I = 9$) and number of experiments ($J = 4$), respectively.

3. Results and Discussion

The irradiance and fluence rate at the reactor light entrance wall were evaluated using the LSSE, LSDE and ESDE light emission models and these were further used in the SFM as boundary conditions. The results were then compared with the full solution of the RTE by DOM using the ESDE model to provide the most accurate solution. Then, the intrinsic kinetic constants of photocatalytic degradation of 2-HBA in P25 TiO_2 suspension were calculated using both methods by solving the species and fluid-dynamics transport equations.

The computational time for the RTE-DOM model was approximately 10 min for each wavelength evaluated, using 4 processors Intel®Core™ i7, while it was instantaneous for the RTE-SFM. The fluid dynamics in the annular reactor were computed in approximately 5 min and the species transport equations in approximately 20 minutes to model 4 hours of experimental reactor time.

3.1. Evaluation of boundary condition for SFM

The SFM requires the evaluation of the incident photon flux, E_0, at the light entrance wall (SFM boundary condition). In literature this has been represented as either irradiance or fluence rate. The irradiance (E_p) [W m^{-2}] and fluence rate ($E_{p,o}$) [W m^{-2}] for collimated

beams perpendicular to the reactor wall are identical. However, in all other cases, irradiance and fluence rate differ as shown by their definitions (Eq. 24-25).

$$\mathrm{E_p} = \int_{2\pi} I \cos(\theta)\ d\Omega \tag{25}$$

$$\mathrm{E_{p,o}} = \int_{4\pi} I\ d\Omega \tag{26}$$

where I is the radiation intensity [W m^{-2} sr^{-1}], θ is the angle between the photon beam and the normal vector to the surface and $d\Omega$ is the differential solid angle.

The fluence rate takes into consideration the intensity of the incident radiation arriving from all directions in the 4π space, whilst the irradiance considers only the intensity of the incident radiation normal to the wall. The SFM has been mostly applied using the fluence rate [14, 18, 23] as incident photon flux, however, irradiance should also be considered as an appropriate boundary condition to solve the SFM. The impact of these two boundary conditions is investigated here, particularly with regards to the calculation of the LVRPA and the intrinsic reaction kinetics constant of photocatalytic oxidation of water contaminants.

The irradiance as boundary condition in the SFM has the advantage to be energy conservative, in contrast, fluence rate gives a better prediction of photon flux seen by the absorber, since the LVRPA is directly proportional to fluence rate (See Eq. (10)). Fig. 1 shows the comparison between irradiance (dashed lines) and fluence rate (solid line) calculated at the inner wall of two photoreactors geometries (Table 1), using the LSSE, LSDE and ESDE emission models.

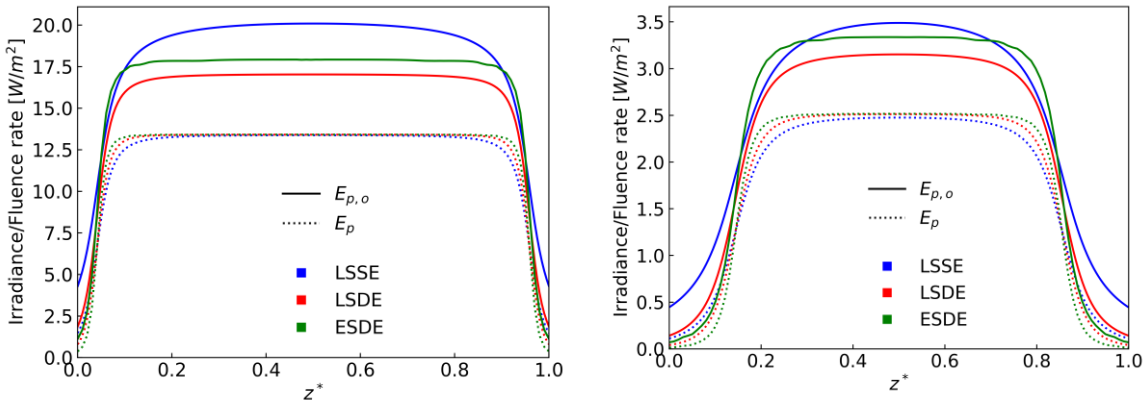

(a) (b)

Fig. 1. UVA irradiance (E_p) and Fluence Rate ($E_{p,o}$) at the light entrance wall of the reactor as a function of dimensionless length. (a) Reactor A, (b) Reactor C.

The maximum irradiance, which is located at the axial center of the photoreactor, differed by up to 40% from the fluence rate. The irradiance profiles at the inner wall of the reactor were slightly affected by the light emission models, however, the fluence rate profiles were highly influenced by these. Light sources that cannot be approximated as line sources relative to the reactor dimensions, extensive source models provide a more accurate representation of the light emitted by the source [28], thus the ESDE model was used here to compare the LVRPA profiles, the TRPA values and the intrinsic reaction kinetics constants of the photocatalytic oxidation of 2-HBA.

3.2. Radiation field in an annular photocatalytic reactor by DOM and SFM

Reactor A configuration in Table 1 was used to illustrate the impact of radiation model on the LVRPA profiles as a function of optical thickness. The RTE was solved with the DOM and with the SFM using either irradiance (SFM(E_0=E_p)) or fluence rate (SFM(E_0 = $E_{p,o}$)) as boundary condition. The optical thickness was varied between 1.8 and 3.2 by changing the catalyst concentration, since this range provides an optimum irradiation of the

285 reactor volume [23]. The results shows (Fig. 2) that the SFM(E_0=E_p) provides a better match
286 to the DOM solutions, in comparison with SFM(E_0 = $E_{p,o}$).

287 The LVRPA close to the inner reactor wall was slightly underpredicted by the
288 SFM(E_0=E_p) since the DOM solution, unlike the SFM, also accounted for the inner wall back
289 scattered photons to be recaptured elsewhere in the annular reactor. In contrast, the
290 SFM(E_0=$E_{p,o}$) overpredicted the LVRPA at the inner wall, since fluence rate was
291 significantly higher than irradiance (Fig. 1). The TRPA was calculated using the
292 SFM(E_0=E_p), the SFM(E_0=$E_{p,o}$) and the DOM solutions of the RTE. The SFM(E_0=E_p)
293 deviated from the DOM solutions by +3.1 to +8.9% in the optical thickness range between
294 1.8 and 3.2, while the SFM(E_0=$E_{p,o}$) deviated by +21 and +29% (Table S1, SI). Thus,
295 irradiance as boundary conditions for the SFM seems to be the most accurate for evaluating
296 the LVRPA.

297 Close examination of the LVRPA axial profiles in the regions near the axial ends of
298 the photoreactor (Fig. 2, z^* between 0.0-0.2 and 0.8-1.0) shows that the SFM(E_0=$E_{p,o}$) gives a
299 better approximation of the LVRPA than the SFM(E_0=$E_{p,}$), when compared to DOM results.
300 Overall, the DOM provides the most accurate solution since the incident photons can also
301 travel in the axial direction of the reactor.

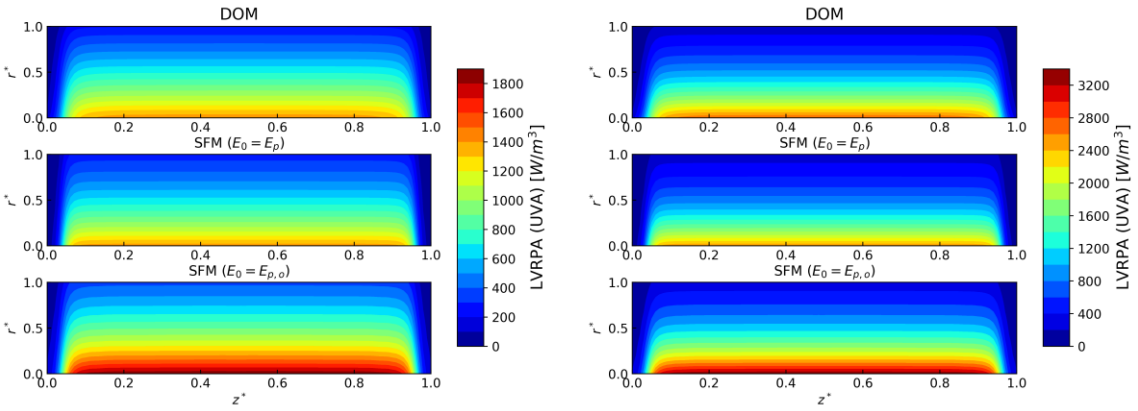

(a) τ = 1.81 (b) τ = 3.18

Fig. 2. LVRPA profiles with DOM, SFM(E_0=E_p) and SFM(E_0=$E_{p,o}$) for reactor configuration A.

The small deviation of TRPA up to 9% in comparison with the DOM results, indicates that the SFM can be used to model annular photoreactors irradiated by diffused light, using irradiance as boundary condition. However, a recent study using an idealized photocatalytic reactor with a cubic geometry irradiated by diffuse light [11], showed much large errors (higher than 120%). This apparent contradiction in findings, may be explained by the inappropriate choice of a cubical photocatalytic reactor [11] which does not present lateral symmetry and thus does not match the assumptions of the SFM [10,14]. The SFM should be applied to geometries with lateral symmetry such as slabs [29], falling-films [23, 30] or annular photoreactors [15, 17], or to geometries irradiated predominantly by collimated light, such as compound parabolic collectors (CPC) [9, 31] used in solar photocatalytic applications. Although it is recognized that the SFM is an analytical approximation of the RTE, the results here presented shows that the SFM remains a very useful tool to model the radiation field in photocatalytic reactors.

3.3. Evaluation of intrinsic kinetic constants of photocatalytic degradation of 2-HBA

The intrinsic reaction kinetics constants of 2-HBA photocatalytic oxidation were evaluated in experimental, annular, flow-through reactors (Reactors A-D, Table 1) by fitting the model predictions to the experimental results reported in [17]. The reactors were operated with radiation sources emitting UVA and UVB radiation, and at very high optical thicknesses ($\tau_{UVA} = 9.5$ and $\tau_{UVB} = 10.7$). The LVRPA profiles for these experimental conditions evaluated using the DOM, the SFM(E_0=E_p)) and the SFM($E_0 = E_{p,o}$) (Fig. S4, SI) show that the radiation field in the reactor was sub-optimal since for $r^* > 0.5$ the reactor was essentially under darkness.

Despite the evident differences shown by the LVRPA profiles (Fig. S4, SI) and TRPA values (Table S2, SI) and the use of the ESDE light source model, the intrinsic reaction kinetics constants of the photocatalytic oxidation of 2-HBA using DOM, SFM(E_0=E_p) and SFM(E_0=$E_{p,o}$) did not vary significantly (Table 2). The constant k_1 estimated by the SFM(E_0=E_p) was only 1% higher than the value with the DOM, and K_{L-H} was 0.8% lower, while those estimated using the SFM(E_0=$E_{p,o}$) were 18% lower and 1.3% higher, respectively. It should be observed that reactor geometry, optical properties and optical thickness would also affect the accuracy of these estimation by SFM and that for other reactor configurations the deviations from the DOM may vary.

Table 2. Intrinsic kinetic constants of 2-HBA photocatalytic oxidation using DOM, and SFM using either irradiance or fluence rate as boundary condition.

Model	$k_1 \cdot 10^{10}$ [kmol m^{-1} s^{-1} W$^{-0.5}$]	$K_{L-H} \cdot 10^{-4}$ [m^3 kmol^{-1}]	R^2
SFM(E_0=E_p)	1.838	2.300	0.955
SFM(E_0=$E_{p,o}$)	1.497	2.349	0.955
DOM	1.820	2.319	0.957

Fig. 3 shows the concentration of 2-HBA as a function of time in the recirculation tank of the system modeled using DOM, SFM(E_0=E_p) and SFM(E_0=$E_{p,o}$), and the comparison with the experimental results [17]. These model simulations were performed using the DOM kinetic constants in Table 2 to highlight the accuracy of the of the SFM model predictions. As expected, the 2-HBA concentration profiles modeled with the SFM(E_0=$E_{p,o}$) deviated from the DOM results, while SFM(E_0=E_p) provided a much closer match. The larger deviations observed in reactor configuration C and D could be ascribed to experimental errors.

The kinetics parameters of 2-HBA photocatalytic degradation using CFD (Table 2) differed slightly from those reported in [17] using streamline flow modeling. Overall, CFD provides a more powerful tool for the modeling of photocatalytic reactors and for a more accurate evaluation of the intrinsic kinetics constants of water contaminants. However, this study shows that the SFM(E_0=E_p) estimated the intrinsic kinetics constants of 2-HBA with accuracy similar to the DOM.

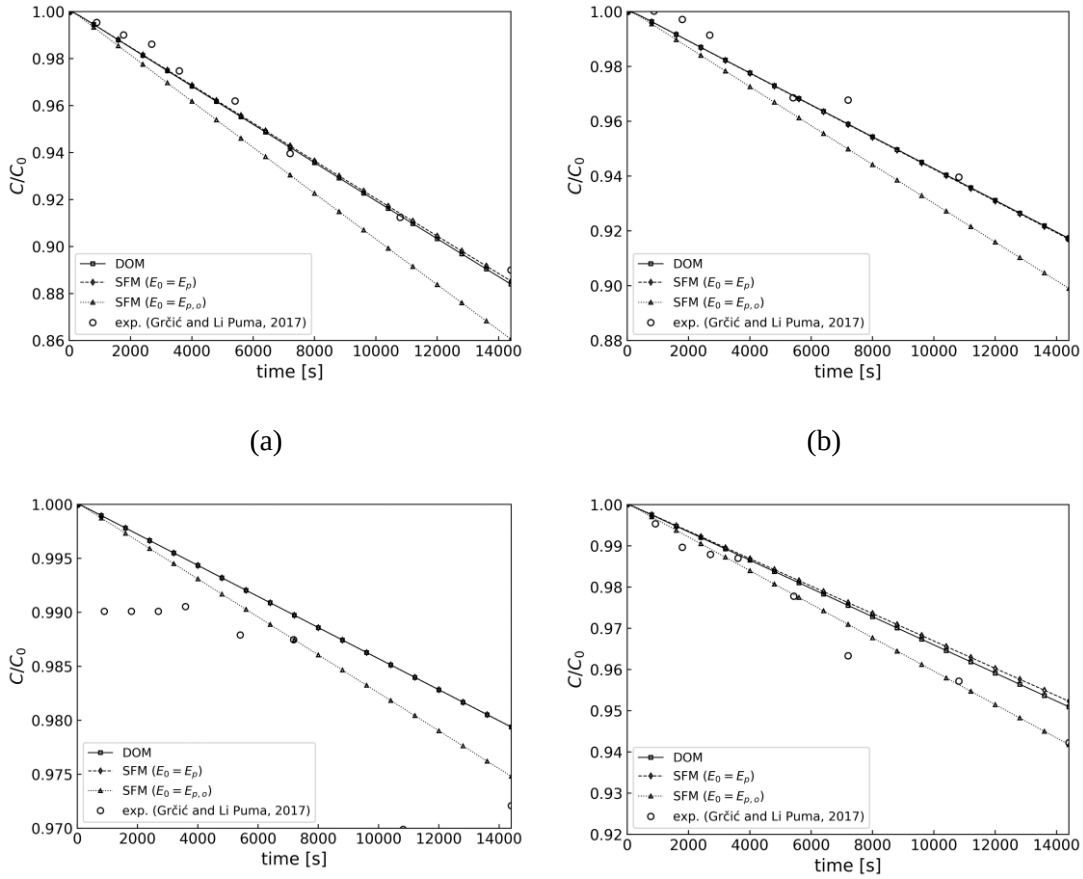

353 **Fig. 3.** Dimensionless concentration of 2-HBA at the recycling tank as a function of
354 time for (a) Reactor A, (b) Reactor B, (c) Reactor C and (d) Reactor D, calculated using
355 DOM, SFM(E_0=E_p) and SFM(E_0=$E_{p,o}$) and comparison with experimental results.

356 **4. Conclusions**

357 In this study, we have shown the importance of modeling photocatalytic reactors by
358 coupling radiation transport, fluid dynamics and reaction kinetics, in order to compute
359 intrinsic reaction kinetics constant of photocatalytic oxidation of water contaminants. CFD
360 modelling provides a more accurate evaluation of the fluid-dynamics in the reactor, and
361 DOM a more accurate evaluation of the radiation field. However, we have shown that the
362 SFM solved with the irradiance boundary condition provides a very close approximation of
363 the radiation field, and a closer approximation than the SFM solved with fluence rate as
364 boundary condition. The SFM also provided a close evaluation of the LVRPA using the

ESDE light emission model. The total rate of photon absorption calculated using the SFM with irradiance boundary condition deviated from the DOM solution by only +3.1 to +8.9%, in the optical thickness range between 1.8 and 3.2. The estimation of the intrinsic reaction kinetics constants of photocatalytic oxidation of 2-HBA in an experimental reactor by SFM and DOM deviated by only 1%. The most significant advantage of the SFM over the DOM is that solutions can be generated instantaneously in a personal computer, while the DOM computational time takes a minimum of 20 min in parallel processing, and this is even more important in solar photocatalytic reactors with ever changing solar irradiance.

Acknowledgements

This study was financed in part by the Coordenação de Aperfeiçoamento de Pessoal de Nível Superior (CAPES), Brazil (Finance Code 001). The authors also acknowledge iESSS (ESSS Institute for Education, Research and Development) for providing the software license to run ANSYS CFD package.

Nomenclature

a	Six Flux Model parameter
b	Six Flux Model parameter
c_{cat}	Catalyst concentration [kg m^{-3}]
C_{2-HBA}	Molar concentration of 2-HBA [kmol m^{-3}]
$D_{i,m}$	Mass diffusivity of specie k in the mixture m [m^2 s^{-1}]
E_w	Irradiance at lamp wall [W m^{-2}]
E_0	Incident photon flux [W m^{-2}]
E_p	Irradiance [W m^{-2}]

$E_{p,o}$	Fluence rate [W m^{-2}]
I	Radiation intensity [W m^{-2} sr^{-1}]
I_b	Black body emission [W m^{-3}]
k_1	kinetic constant in [kmol m^{-1} s^{-1} $W^{-0.5}$]
K_{L-H}	Langmuir-Hinshelwood binding constant [m^3 $kmol^{-1}$]
N	Number of chemical species
N_θ	Number of angular discretizations in θ
N_ϕ	Number of angular discretizations in ϕ
m	Order of reaction related to the LVRPA
p_f	Forward scattering probability coefficient
p_b	Backward scattering probability coefficient
p_s	Sideward scattering probability coefficient
P	Pressure [Pa]
Q	Volumetric flow rate [m^3 s^{-1}]
r	Radial coordinate [m]
r^*	Dimensionless radial coordinate
r_{2-HBA}	Reaction rate in [kmol m^{-3} s^{-1}]
R	External radius [m]
R_i	Source of Y_i in mass transport equation [kg m^{-3} s^{-1}]
R_{int}	Internal radius [m]
R_L	Lamp radius [m]
t	Time [s]
T	Temperature [K]
$\boldsymbol{u}$	Velocity [m s^{-1}]
V_{tank}	Volume of the tank [L]

V_w	Molar volume of water [m^3 mol^{-1}]
V_{2-HBA}	Molar volume of 2-HBA [m^3 mol^{-1}]
Y_i	Mass fraction of specie k
z	Axial coordinate [m]
z^*	Dimensionless axial coordinate
Greek letters	
γ	Parameter of Six Flux Model
ε	Emissivity
η	Ratio between internal and external radius
θ	Polar coordinate
κ^*	Specific absorption coefficient [m^2 kg^{-1}]
λ	Wavelength [nm]
μ	Viscosity [Pa s]
ρ	Density [kg m^{-3}]
σ^*	Specific averaged scattering coefficient [m^2 kg^{-1}]
τ	Optical thickness
τ_{app}	Apparent optical thickness
ϕ	Azimuthal angle
ω	Scattering albedo
ω_{corr}	Corrected scattering albedo
$\Phi(\vec{s} \rightarrow \overrightarrow{s'})$	Scattering phase function
Ω	Solid angle
Abbreviations	

CFD	Computational Fluid Dynamics
DOM	Discrete Ordinates Model
exp	Experimental
ESDE	Extensive source superficial diffuse emission
LVRPA	Local volumetric rate of photon absorption
LSDE	Line source diffuse emission
LSSE	Line source spherical emission
RTE	Radiation Transport Equation
SFM	Six Flux Model
SFM(E_0=E_p)	Six-Flux Model using the irradiance profile as incident photon flux
SFM(E_0=$E_{p,o}$)	Six-Flux Model using the fluence rate profile as incident photon flux
TRPA	Total rate of photon absorption
2-HBA	2-hydroxybenzoic acid

381

382

383 **References**

384

1] D. D. Dionysiou, G. Li Puma, J. Ye, J. Schneider, D. Bahnemann, Photocatalysis: Applications, RSC Energy and Environmental Series, Royal Society of Chemistry, 2016.

2] S. K. Loeb, P. J. J. Alvarez, J. A. Brame, E. L. Cates, W. Choi, J. Crittenden, D. D. Dionysiou, Q. Li, G. Li-Puma, X. Quan, D. L. Sedlak, T. D. Waite, P. Westerhoff, J.-H. Kim, The Technology Horizon for Photocatalytic Water Treatment: Sunrise or Sunset?, Environ. Sci. Technol. 53 (2019) 2937-2947.

A. E. Cassano, O. M. Alfano, Reaction engineering of suspended solid

3] heterogeneous photocatalytic reactors, Catal. Today 58 (2000) 167-197.

M. L. Satuf, R. J. Brandi, A. E. Cassano, O. M. Alfano, Photocatalytic
4] degradation of 4-chlorophenol: A kinetic study, App. Catal. B: Environ. 82 (2008) 37-49.

C. Casado, J. Marugán, R. Timmers, M. Muñoz, R. van Grieken, Comprehensive
5] multiphysics modeling of photocatalytic processes by computational fluid dynamics based on intrinsic kinetic parameters determined in a differential photoreactor, Chem. Eng. J. 310 (2017) 368-380.

Y. Boyjoo, M. Ang, V. Pareek, Some aspects of photocatalytic reactor modeling
6] using computational fluid dynamics, Chem. Eng. Sci. 101 (2013) 764-784.

A. Turolla, D. Santoro, J. de Bruyn, F. Crapulli, M. Antonelli, Nanoparticle
7] scattering characterization and mechanistic modelling of UV-TiO_2 photocatalytic reactors using computational fluid dynamics, Water Res. 88 (2016) 117-126.

P. J. Coelho, Advances in the discrete ordinates and finite volume methods for
8] the solution of radiative heat transfer problems in participating media, J. Quant. Spectrosc. Rad. Transfer 145 (2014) 121-146.

R. Acosta-Herazo, J. Monterroza-Romero, M. Á. Mueses, Coupling the Six Flux
9] Absorption–Scattering Model to the Henyey-Greenstein scattering phase function: Evaluation and optimization of radiation absorption in solar heterogeneous photoreactors, Chem. Eng. J. 302 (2016) 86-96.

A. Brucato, A. E. Cassano, F. Grisafi, G. Montante, L. Rizzuti, G. Vella,
10] Estimating Radiant Fields in Flat Heterogeneous Photoreactors by the Six-Flux Model, AICHE J. 52 (2006) 3882-3890.

M. A. Ramírez-Cabrera, P. J. Valadés-Pelayo, C. A. Arancibia-Bulnes, E.

11] Ramos, Validity of the Six-Flux model for photoreactors, Chem. Eng. J. 330 (2017) 272-280.

12] A. Brucato, L. Rizzuti, Simplified Modeling of Radiant Fields in Heterogeneous Photoreactors. 1. Case of Zero Reflectance, Ind. Eng. Chem. Res. 36 (1997) 4740-4747.

13] A. Brucato, L. Rizzuti, Simplified Modeling of Radiant Fields in Heterogeneous Photoreactors. 2. Limiting "Two-Flux" Model for the Case of Reflectance Greater Than Zero, Ind. Eng. Chem. Res. 36 (1997) 4748-4755.

14] G. Li Puma, A. Brucato, Dimensionless analysis of slurry photocatalytic reactors using two-flux and six-flux radiation absorption–scattering models, Catal. Today 122 (2007) 78-90.

15] E. Mena, A. Rey, F. J. Beltrán, TiO_2 photocatalytic oxidation of a mixture of emerging contaminants: A kinetic study independent of radiation absorption based on the direct indirect model, Chem. Eng. J. 339 (2018) 369-380.

16] J. Marugán, R. van Grieken, A. E. Cassano, O. M. Alfano, Intrinsic kinetic modeling with explicit radiation absorption effects of the photocatalytic oxidation of cyanide with TiO_2 and silica-supported TiO_2 suspensions, App. Catal. B: Environ. 85 (2008) 48-60.

17] I. Grčić, G. Li Puma, Six-flux absorption-scattering models for photocatalysis underwide-spectrum irradiation sources in annular and flat reactors using catalysts with different optical properties, App. Catal. B: Environ. 211 (2017) 222–234.

18] I. Grčić, G. Li Puma, Photocatalytic Degradation of Water Contaminants in Multiple Photoreactors and Evaluation of Reaction Kinetic Constants Independent of Photon Absorption, Irradiance, Reactor Geometry, and Hydrodynamics, Environ. Sci. Technol. 47 (2013) 13702-13711.

J. Colina-Márquez, F. Machuca-Martínez, G. Li Puma, Photocatalytic
19] Mineralization of Commercial Herbicides in a Pilot-Scale Solar CPC Reactor: Photoreactor Modeling and Reaction Kinetics Constants Independent of Radiation Field, Environ. Sci. Technol. 43 (2009) 8953-8960.

G. Camera-Roda, V. Augugliaro, A. G. Cardillo, V. Loddo, L. Palmisano, F.
20] Parrino, F. Santarelli, A reaction engineering approach to kinetic analysis of photocatalytic reactions in slurry systems, Catal. Today 259 (2015) 87-96.

ANSYS, "ANSYS Documentation, Release 19," ANSYS, 2018. [Online].
21] Available: https://ansyshelp.ansys.com/. [Accessed 2019].

M. J. O'Neil, The Merck Index: An Encyclopedia of Chemicals, Drugs, and
22] Biologicals (14th ed.), New Jersey: Merck (2006).

G. Li Puma, Modeling of Thin-Film Slurry Photocatalytic Reactors Affected by
23] Radiation Scattering, Environ. Sci. Technol. 37 (2003) 5783-5791.

E. R. Blatchley III, Numerical modelling of UV intensity: application to
24] collimated-beam reactors and continuous-flow systems, Water Res. 31 (1997) 2205-2218.

T. Akehata, T. Shirai, Effect of light-source characteristics on the performance of
25] circular annular photochemical reactor, J. Chem. Eng. Japan 5 (1972) 385-391.

T. Yokota, T. Iwano, T. Tadaki, Light intensity in an annular photochemical
26] reactor, Kagaku Kogaku Ronbunshu 2 (1976) 298-303.

G. Camera-Roda, V. Loddo, L. Palmisano, F. Parrino, Guidelines for the
27] assessment of the rate law of slurry photocatalytic reactions, Catal. Today 281 (2017) 221-230.

J. E. Duran, F. Taghipour, M. Mohseni, Irradiance modeling in annular

28] photoreactors using the finite-volume method, J. Photochem. Photobiol. A: Chem. 215 (2010) 81-89.

29] R. Acosta-Herazo, M. Á. Mueses, G. Li Puma, F. Machuca-Martínez, Impact of photocatalyst optical properties on the efficiency of solar photocatalytic reactors rationalized by the concepts of initial rate of photon absorption (IRPA) dimensionless boundary layer of photon absorption and apparent optical thickness, Chem. Eng. J. 356 (2019) 839-849.

30] J. Colina-Marquez, D. Castilla-Caballero, F. Machuca-Martinez, Modeling of a falling-film photocatalytic reactor: Fluid dynamics for turbulent regime, Appl. Math. Model. 40 (2016) 812-821.

31] H. L. Otálvaro-Marín, F. González-Caicedo, A. Arce-Sarria, M. A. Mueses, J. C. Crittenden, F. Machuca-Martinez, Scaling-up a heterogeneous H_2O_2/TiO_2/solar-radiation system using the Damköhler number, Chem. Eng. J. 364 (2019) 244-256.

385

386

Supplementary Information (SI)

Click here to download Data in Brief: SupplementaryInformation.docx

***Credit Author Statement**

Rodrigo PERALTA MUNIZ MOREIRA: Methodology, Investigation, Conceptualization, Software, Validation, Formal Analysis, Writing – Original Draft

Gianluca LI PUMA: Supervision, Conceptualization, Writing-Review & Editing